ELSEVIER

Biophysical Chemistry 71 (1998) 205–220

Biophysical Chemistry

Near UV circular dichroism from biomimetic model compounds define the coordination geometry of vanadate centers in MeVi- and MeADPVi-rabbit myosin subfragment 1 complexes in solution

Katalin Ajtai [a], Fang Dai [a], Sungjo Park [a], Carlos R. Zayas[a 1], Y. Michael Peyser [b], Andras Muhlrad [b], Thomas P. Burghardt [a,*]

[a] *Department of Biochemistry and Molecular Biology, Mayo Foundation, Rochester, MN 55905, USA*
[b] *Department of Oral Biology, Hebrew University, Jerusalem 91120, Israel*

Received 24 September 1997; revised 8 January 1998; accepted 8 January 1998

Abstract

The circular dichroism (CD) spectrum was measured from vanadate (Vi) cyclic esters of chiral vicinal diols, hydroxycarboxylates, and cyclodextrines as a function of Vi concentration ([Vi]) and at the lowest energy transitions of the vanadium. At low [Vi] and in the presence of excess vicinal diols, hydroxycarboxylates, or cyclodextrines the CD signal intensity scales linearly with [Vi] indicating the predominance of a monomeric cyclic ester. At higher [Vi], the signal intensity in the presence of the vicinal diols and hydroxycarboxylates become nonlinear in [Vi], indicating formation of a dimeric cyclic ester. Vanadium-51 NMR (^{51}V-NMR) indicates the coordination geometry of several of these model Vi centers in solution and identifies the CD signals characteristic to Vi trigonal bipyramidal (tbp) and octahedral (Oh) coordination geometries from monomeric and dimeric species. The CD spectra from monomeric and dimeric forms of the tbp-coordinated model compounds have two apparent transitions with amplitudes of opposite sign at wavelengths $\geq$ 240 nm. Spectra from the monomeric and dimeric Oh coordinated species are distinct from the tbp-type spectra over the same wavelength domain because of the presence of two additional transitions with opposite sign amplitudes. These model spectra were compared to the vanadate CD spectra from Vi bound to rabbit myosin subfragment 1 (S1) in solution, in the presence of divalent metal cations (MeVi-S1) or trapped with MeADP (MeADPVi-S1). Polymeric MeVi binds to the active site of S1 and the vanadate centers in MnVi-S1 or CoVi-S1 produce a CD signal resembling that from the tbp model. The trapped

Abbreviations: ADP, Adenosine diphosphate; AlF_4^-, Aluminum fluoride; BeF_x, Beryllium fluoride; CD, Circular dichroism; CI, Configuration interaction; DTT, Dithiothreitol; Me, Divalent metal cation; MeADPVi-S1, MeADPVi-trapped myosin subfragment 1; MeVi-S1, MeVi-bound myosin subfragment 1; Oh, Octahedral; S1, Myosin subfragment 1; SDS-PAGE, Sodiumdodecylsulfate polyacrylamide gel electrophoresis; SH1, Fast reacting thiol of myosin subfragment 1; tbp, Trigonal bipyramidal; Td, Tetrahedral; Trp510, Tryptophan 510 in rabbit myosin subfragment 1; UV, Ultraviolet; V, Vanadium; Vi, Orthovanadate in oxidation state (V); ^{51}V-NMR, Vanadium-51 nuclear magnetic resonance

* Corresponding author.
[1] Present address: University of Puerto Rico, School of Medicine, Rio Piedras, Puerto Rico 00931, USA.

PII S0301-4622(98)00097-0

ATPase transition state analog MeADPVi produces a different CD signal resembling that from the Oh model.

Keywords: γ-Phosphate coordination geometry; Transient state analog; Energy transduction; Trigonal bipyramidal; Octahedral; Vanadate coordination in myosin

1. Introduction

The energy causing the relative translation of myosin and actin filaments during muscle contraction originates from the free energy released by the breaking of ATP's γ-phosphate bond in ATP hydrolysis. The myosin cross-bridge or subfragment 1 (S1) contains the energy transducer needed to convert the chemical free energy to work. The free energy exchange between ATP and myosin may occur during communication of the progressive change in γ-phosphate structure to the S1 active site structure, in analogy with the mechanism proposed for other ATPases [1]. We showed earlier that the distance from the γ-phosphate atom, P_γ, to the oxygen connecting the γ- and β-phosphates, is an important characteristic of the ATP transition state structure [2]. Differing coordination geometries of the P_γ with its oxygen ligands, starting with tetrahedral (Td) and ending with trigonal bipyramidal (tbp) [1], also characterize the transition structures. The work presented here regards the coordination geometry aspect of the structural characterization of P_γ during hydrolysis.

Studies of model compounds showed that inorganic phosphate can form Td, octahedral (Oh), square pyramidal, and tbp coordination geometries [1,3,4], giving a set of possibilities to consider for transition state structures during ATP hydrolysis. In recent years, the phosphate analog vanadate (Vi), beryllium fluoride (BeF_x), aluminum fluoride (AlF_4^-), and scandium fluoride that stabilize the various intermediates of myosin-catalyzed ATP hydrolysis, were increasingly used to characterize these intermediates [5–13]. The crystallographic structures of MgADP beryllium fluoride ($MgADPBeF_x$), aluminum fluoride ($MgADPAlF_4^-$), or vanadate (MgADPVi) trapped truncated *Dictyostelium* S1 identified the coordination geometry of the phosphate analogs [14,15]. The observed Td, Oh, and tbp structures of the phosphate analog complexes, and other properties associated with trapped S1 that are unique for each analog including: (i) the fluorescence intensity from the ATP sensitive tryptophan [8], (ii) the shape of the probe binding cleft containing tryptophan 510 (Trp510) and the fast reacting thiol (SH1) [16], (iii) the reactivity of SH1 [17], and (iv) the near ultra violet (UV) circular dichroism (CD) spectrum [12], all suggest that the trapped phosphate analog S1, in some important respects, represents the structure of the different transition states. The suggestion of tbp coordinated vanadate in crystallized MgADPVi trapped S1 [15] agrees with findings from other Vi-trapped enzymes [18].

We used spectroscopic methods to investigate the coordination geometry of the vanadate center in MeADPVi trapped rabbit S1 (MeADPVi-S1), and Vi bound to S1 without ADP (MeVi-S1), in solution and in the presence of various divalent metal cations (Me). The lowest energy absorption bands of Vi occur in the near UV spectrum at a lower energy than the protein absorption band permitting selective observation of Vi absorption. The CD spectra measured from model Vi structures in solution, containing either tbp [19–23] or Oh [24] coordination geometries, are compared to similar signals originating from MeADPVi-S1 and MeVi-S1. The model CD signals provide a spectroscopic fingerprint differentiating the tbp and Oh coordination of the vanadate. The CD signals from Vi in S1 also differentiate between the Vi structures in MeVi-S1 and MeADPVi-S1, suggesting that the vanadate centers in MeADPVi-S1 and MeVi-S1 coordinate in the Oh and tbp geometries, respectively. These findings differ from that observed for truncated *Dictyostelium* S1, perhaps reflecting differences between crystallized and solution forms of the S1 structure, and/or, truncated *Dictyostelium* and rabbit S1 structure [25,26]. These findings also raise questions about the relevance of the coordination of vanadium (V) as a phosphate analog, and how the trapped vanadate fits into the transition state kinetics scheme of myosin ATPase.

2. Materials and methods

2.1. Chemicals

R(−)- and *S*(+)-propanediol, and, *R*(−)- and *S*(+)-lithium-lactate were from Fluka (Ronkonkoma, NY). Vanadate, Tris, HEPES, ATP, ADP, phenylmethanesulfonyl fluoride (PMSF), α-chymotrypsin, ethylenediaminetetraacetic acid (EDTA), dithiothreitol (DTT), α- and β-cyclodextrin were from Sigma (St. Louis, MO). All chemicals were analytical grade.

2.2. Solutions

A stock solution of sodium vanadate was made by the method of Goodno [27].

2.3. Preparation of model compounds

Chiral cyclic esters of Vi with *R*- or *S*-propanediol were prepared in 50 mM Tris–HCl buffer at pH 7.5 according to Gresser and Tracey [19]. Vanadate and propanediol concentrations varied from 0.0125–1.0 mM and 0.02–2.63 M, respectively, depending on the experiment. Chiral cyclic esters of Vi with *R*- or *S*-lactate were prepared in 1 M KCl and 10 mM Tris–HCl at pH 7.5 or 7.35, or, HEPES buffer at pH 6.1 according to Tracey et al. [24]. Vanadate and lactate concentrations varied from 0.025–1.0 mM and 0.075–0.10 M, respectively, depending on the experiment. Vanadate cyclodextrin complexes were formed at 6.2–100 μM vanadate and 10 mM α- or β-cyclodextrin in 25 mM TES at 4°C and pH 6 or 7.

2.4. Preparation of myosin S1, MeADPVi-S1, and MeVi-S1

We prepared rabbit myosin by a standard method [28] and S1 by digesting myosin filaments with α-chymotrypsin [29]. MeADPVi-S1 complexes were formed by incubating 20 μM S1 in 50 mM KCl and 25 mM HEPES buffer at pH 7.0 with 100 μM ADP and chloride salts of divalent metals. The concentration of the metal chlorides contained 0.5 mM Mg^{2+}, 0.2 mM Mn^{2+}, 0.2 mM Fe^{2+}, 0.2 mM Co^{2+}, 0.2 mM Ni^{2+}, or 0.5 mM Ca^{2+}. The trapped S1 complexes were formed by incubating S1 at 20°C with ADP and $MeCl_2$ for 5 min. Subsequently, 0.2 mM vanadate was added and the samples incubated for 5–20 min. When necessary, free reagents were removed from the samples by gel filtration on a Sephadex PD10 column (Pharmacia, Uppsala, Sweden).

MeVi-S1 complexes were formed identically to the MeADPVi-S1 complexes at vanadate concentrations of 0.2, 0.5, 1.0 mM, but without ADP and using 1 mM divalent metal.

2.5. Vanadate-induced photocleavage of S1

Experiments were carried out on 8 μM S1 in the presence of 0.5 mM Vi, 0.5–5.0 mM $MnCl_2$ or $CoCl_2$, and 30 mM HEPES at pH 7.0. Protein samples on ice were irradiated by a UV transilluminator emitting 365 nm for 10 min [30].

2.6. Sodiumdodecylsulfate polyacrylamide gel electrophoresis (SDS-PAGE)

SDS-PAGE was performed on 7–18% polyacrylamide gradient slab gels. Molecular masses of the bands were estimated by comparing the electrophoretic mobility of the bands with that of authentic markers.

2.7. Spectroscopic measurements

We measured absorption spectra on a Beckman DU650 (Beckman Instruments, Fullerton, CA) spectrophotometer and CD spectra on a Jasco J720 spectropolarimeter (Jasco, Tokyo, Japan). All CD measurements were made at 4°C with spectral resolution of 2 nm.

The CD spectra from the model compounds were recorded in the 240–400 nm wavelength domain, where only the complexed vanadate center contributes. Free vanadate, propanediol, lactate, or cyclodextrin have no measurable CD signal on this wavelength domain for the concentrations used in the optical experiments.

The CD spectra from MeADPVi-S1 and MeVi-S1 were recorded in the 250–400 nm wavelength domain, where ADP and S1 contribute appreciable CD signals at wavelengths $\leq$ 300 nm. Subtracting spectra

from identically prepared samples with and without vanadate isolated the CD spectrum of the vanadate center from the total signal.

2.8. Curve fitting

We used the sum of four Gaussian curves to fit the CD spectra and estimate rotary strengths for the lowest energy absorption bands of vanadate. A constrained least squares protocol located the best linear parameters (amplitudes) during curve fitting [31]. The best nonlinear parameters (spectral maxima and widths) were found by grid search.

2.9. Vanadium-51 nuclear magnetic resonance (^{51}V-NMR)

^{51}V-NMR was performed at the Mayo NMR core facility on a Bruker AMX-500 spectrometer operating at 131 MHz. Pulse widths of 60° (40 μs), spectral widths of 25 kHz, and a repetition rate of 5 Hz were used during the 30 000 spectral scans. Chemical shifts are reported relative to $VOCl_3$ via an external reference of Na_3VO_4 in water (-572.9 ppm). All measurements were made at 4°C.

3. Results

3.1. Identification of species in the model systems using NMR

We use a mixture of vanadate with chiral propanediol or lactate to make molecules containing vanadium in the tbp [19–23] or Oh [24] coordination geometry. Earlier work identified the family of molecular species produced in each mixture as a function of several experimental parameters including total vanadate concentration $[Vi]_T$, total propanediol or lactate concentration $[T]_T$, and pH. We use these parameters to study the effect of dimer formation on the CD signal and to control the coordination geometry of the vanadium.

^{51}V-NMR identified the molecular species in our model systems. The ^{51}V-NMR from a mixture of 2.63 M propanediol and 0.5 mM vanadate in Tris–HCl buffer at pH 7.5 produced a spectrum similar to that observed previously [19]. There, two resonance lines near to -521 ppm were assigned to two isomers of a dimeric cyclic ester of vanadate in the tbp coordination. Also detected were resonances from free vanadate and acyclic esters of vanadate. We observed similar NMR spectra for the *R*- or *S*-isomer of the propanediol in mixture with vanadate (data not shown).

The ^{51}V-NMR from a mixture of 100 mM lactate, 1.0 mM vanadate, and 1 M KCl in Tris–HCl buffer at pH 7.5 produced a spectrum similar to that observed previously [24]. There, resonances were assigned to a monomeric cyclic ester of vanadate in the tbp coordination and to free vanadate in monomeric, dimeric, and tetrameric forms. Upon lowering the pH to 7.35, the ^{51}V-NMR from the same mixture produced a spectrum again similar to that observed previously. There, resonances were assigned to cyclic esters of vanadate in tbp (monomeric) and Oh (dimeric) coordination and to free vanadate in monomeric, dimeric and tetrameric forms. Finally, the ^{51}V-NMR spectrum from the same mixture except that the buffer was HEPES at pH 6.1 produced a spectrum indicating the exclusive presence of dimeric cyclic esters of vanadate in the Oh coordination. The NMR spectrum at pH 6.1 was not previously reported, and is shown with the pH 7.35 spectrum for a mixture of vanadate and lactate in Fig. 1. Our assignment of structure in pH 6.1 is based on comparison to the assignments made previously at higher pH. The lowering of pH below 6.1 had no effect on the observed NMR spectrum. We observed identical NMR spectra for the *R*- or *L*- isomer of the lactate in mixture with vanadate.

3.2. Identification of species in the model systems using CD

Only molecules containing cyclic esters are optically active in the lowest energy absorption bands of Vi so that the observed CD signal in mdeg divided by the optical path length in cm, S/ℓ, is given by

$$S/\ell = 32980(\Delta\epsilon_M[M] + \Delta\epsilon_D[D]) \quad (1)$$

where $\Delta\epsilon_M$ and $\Delta\epsilon_D$ are the CD molar extinction coefficients for the monomeric and dimeric cyclic ester of concentrations [M] and [D]. S is measured as a function of excitation wavelength λ.

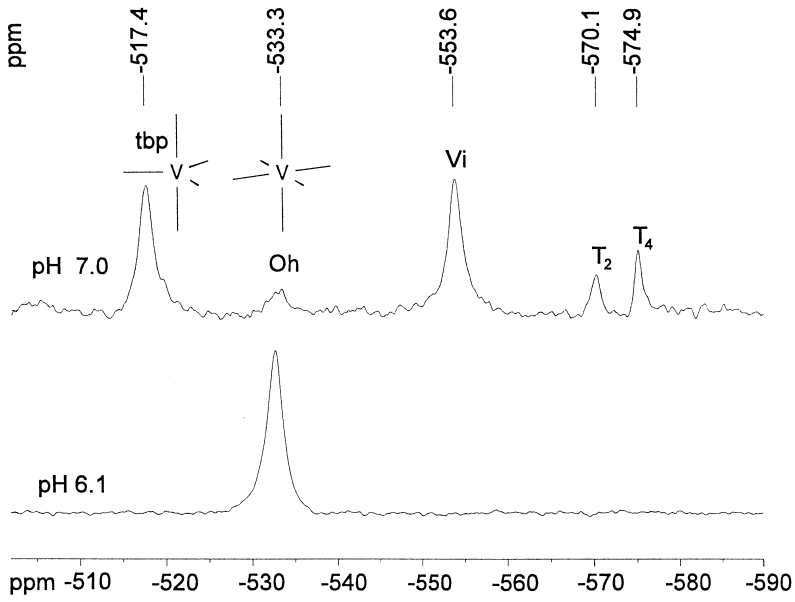

Fig. 1. The ^{51}V-NMR spectrum from 1.0 M KCl, 0.1 M *S*-lactate, 1.0 mM vanadate, and 10 mM Tris–HCl buffer at pH 7.35 (top) or HEPES buffer at pH 6.1 (bottom). The assignment of the chemical species with the resonance peak are indicated, where tbp is trigonal bipyramidal, Oh is octahedral, and, T_2 and T_4 are dimeric and tetrameric vanadate. The tbp-coordinated species is monomeric, while the Oh-coordinated species is dimeric at the Vi concentrations used in these experiments.

We observed CD spectra from the *R*-propanediol–Vi cyclic ester as a function of $[Vi]_T$. The $[Vi]_T$ was varied from 12.5 to 350 μM in the presence of total propanediol concentration, $[T]_T$ = 0.263 M. Fig. 2 shows several of these spectra. The signal intensity vs. $[Vi]_T$ from these data is linear at the lowest concentrations, indicating the predominance of the monomeric cyclic ester species. Signal intensity vs. $[Vi]_T$ at higher concentration is nonlinear and concave upward, indicating dimer formation; however, the shape of the spectra were always independent of $[Vi]_T$. Changing pH did not affect the shape or intensity of the CD signal. The unchanging CD spectral shape during the formation of dimers implies from Eq. (1) that $\Delta\epsilon_M \propto \Delta\epsilon_D$, and that the monomers coordinate in the dimer in a manner that does not alter the energies of the absorption bands. By observing S/ℓ in Eq. (1) as a function of both $[Vi]_T$ and $[T]_T$, we obtained $\Delta\epsilon_M$ and $\Delta\epsilon_D$, shown in Fig. 3, by the method described in Appendix A. The replacement of *R*- with *S*-propanediol in the mixture with vanadate reversed the sign but did not otherwise alter the observed CD. The ^{51}V-NMR data and X-ray crystallographic structure suggest that the dimeric cyclic ester of propanediol–Vi is in the tbp coordination geometry [19,20,22,23]. The shape of the CD spectrum from the propanediol–Vi cyclic ester is bimodal at wavelengths above 240 nm and

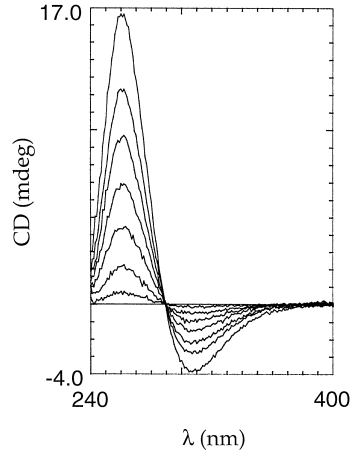

Fig. 2. The CD signal from *R*-propanediol–Vi cyclic esters at pH 7.5 in the tbp coordination geometry for several $[Vi]_T$s and 0.263 M *R*-propanediol. Lowest to highest intensity spectra are plotted for $[Vi]_T$ = 50, 100, 150, 200, 250, 300, and 350 μM in a 1-cm cell.

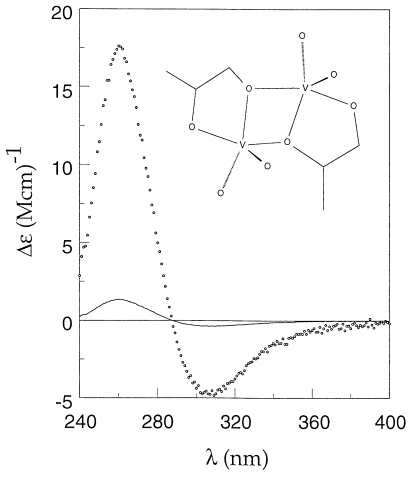

Fig. 3. The monomer $\Delta\epsilon_M$ (solid) and dimer $\Delta\epsilon_D$ (∘ ∘ ∘) CD extinction coefficients for *R*-propanediol–Vi cyclic esters at pH 7.5 in the tbp coordination geometry. The inset shows the observed structure for the dimeric cyclic ester [21,23] giving $\Delta\epsilon_D$.

identical over the range of $[Vi]_T$, where monomeric or dimeric forms are predominant, suggesting that both forms are tbp. The inset in Fig. 3 shows the observed structure for the dimeric cyclic ester [21,23].

The CD spectrum of *R*- or *S*-lactate–Vi was studied at two pH values. We observed CD spectra from the *S*-lactate–Vi cyclic ester at pH 7.5, as a function of $[Vi]_T$. The $[Vi]_T$ was varied from 50 to 500 μM in the presence of total lactate concentration, $[T]_T = 0.20$ M. Fig. 4 shows several of these spectra. At this pH the cyclic lactate–Vi ester was proposed to be monomeric and in the tbp coordination geometry [24]. The observed CD signal intensity scales linearly with $[Vi]_T$ over most of the 50–500 μM domain confirming the predominance of the monomeric species. At the highest $[Vi]_T$s, the shape of the CD spectra depend on $[Vi]_T$, indicating some dimer formation. The spectral shape at all concentrations is similar to that obtained from propanediol–Vi reinforcing the assignment of tbp structure to this species. The replacement of *S*-lactate with *R*-lactate in the mixture reversed the sign but did not otherwise alter the CD signal.

We observed the CD spectra from the *S*-lactate–Vi cyclic ester at pH 6.1, as a function of $[Vi]_T$. The $[Vi]_T$ was varied from 25 to 500 μM in the presence of total lactate concentration, $[T]_T = 0.075$ M. Fig. 5 shows several of these spectra. The CD signal intensity vs. $[Vi]_T$ from these data is linear at the lowest concentrations, indicating the predominance of the monomeric cyclic ester species. At higher $[Vi]_T$, the shape of the CD spectra depend on $[Vi]_T$ indicating dimer formation. By observing S/ℓ in Eq. (1) as a function of $[Vi]_T$ we obtain $\Delta\epsilon_M$ and $\Delta\epsilon_D$ by the method described in Appendix A, and these quantities are shown in Fig. 6. The replacement of *S*-lactate

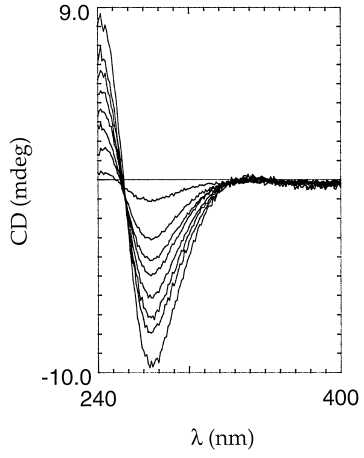

Fig. 4. The CD signal from *S*-lactate–Vi cyclic esters at pH 7.5 in the tbp coordination geometry for several $[Vi]_T$s and 0.20 M *S*-lactate. Lowest to highest intensity spectra are plotted for $[Vi]_T$ = 50, 150, 200, 250, 300, 350, 400, and 500 μM in a 1 cm cell.

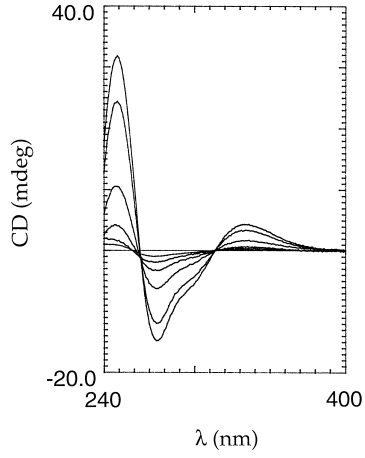

Fig. 5. The CD signal from *S*-lactate–Vi cyclic esters at pH 6.1 in the Oh coordination geometry for several $[Vi]_T$s and 0.075 M *S*-lactate. Lowest to highest intensity spectra are plotted for $[Vi]_T$ = 25, 50, 100, 200, 400, and 500 μM in a 1 cm cell.

with *R*-lactate in the mixture with vanadate reversed the sign, but did not otherwise alter the CD signal. ^{51}V-NMR indicates that the dimeric cyclic ester of lactate–Vi is in the Oh coordination geometry [24]. The CD spectrum from the Oh species has an additional bimodal feature, when compared to the tbp form, that is present over the range of [Vi], where both the monomeric and dimeric forms are predominant, suggesting that both forms are Oh. The inset in Fig. 6 shows the proposed Oh coordinated monomeric cyclic ester.

We used α-(cyclohexaamilose) and β-(cyclooctaamilose) cyclodextrins as chiral templates of Vi. Cyclodextrines are macrocyclic D-glucose oligomers known to produce enantioselective enrichment of racemates [32]. We observed the CD spectra from the α-cyclodextrin–Vi complex at pH 7, as a function of $[Vi]_T$. The $[Vi]_T$ was varied from 6.2 to 100 μM in the presence of 10 mM α-cyclodextrin. Fig. 7 shows several of these spectra. The CD signal intensity vs. $[Vi]_T$ from these data is linear over the entire concentration domain, indicating predominance of a monomeric cyclic ester species. The shape of the spectra are independent of $[Vi]_T$. The absolute signal intensity indicates that cyclodextrin is a more efficient producer of the vanadate cyclic ester than propanediol. An identical signal was produced by the complex at pH 6. The spectra in Fig. 7 and that from the *R*-propanediol–Vi complex have similar shapes that are characteristic to the tbp-coordinated Vi. The interaction of Vi with cyclodextrin is probably through a cyclic esterification reaction involving two vicinal-OH groups of the glucose units. A similar complex was found in the RNase-uridine-Vi crystal, where a cyclic Vi ester was formed between the vicinal OHs of the nucleotide ribose ring [33]. The tbp-coordinated vanadate in the cyclodextrin–Vi model complex demonstrates a new more efficient biomimetic compound for optical and NMR studies of vanadate structure.

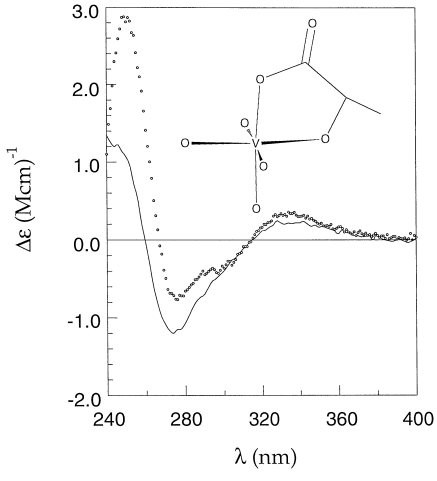

Fig. 6. The monomer $\Delta\epsilon_M$ (solid) and dimer $\Delta\epsilon_D$ (◦ ◦ ◦) CD extinction coefficients for *S*-lactate–Vi cyclic esters at pH 6.1. The inset shows the proposed *S*-lactate–Vi monomeric cyclic ester in the Oh coordination geometry giving $\Delta\epsilon_M$.

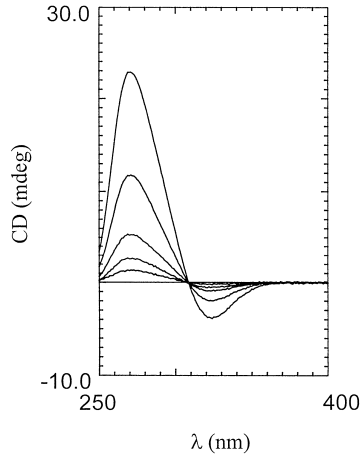

Fig. 7. The CD spectrum of the α-cyclodextrin–Vi complex at pH 7.0 for several $[Vi]_T$s and 10 mM α-cyclodextrin in 25 mM TES at 4°C. Lowest to highest intensity spectra are plotted for $[Vi]_T$ = 6.2, 12.5, 25, 50, and 100 μM in a 1 cm cell.

3.3. CD from MeVi-S1 and MeADPVi-S1

Myosin S1 complexed with MeVi develops a strong extrinsic Cotton effect in the vanadate absorption band. Fig. 8 shows the vanadate center CD spectrum of CoVi-S1. A similar spectrum was observed from MnVi-S1. Results from Section 3.2 above show that the CD spectrum from tbp-coordinated Vi has a characteristic bimodal shape quite different from the spectrum obtained from Oh coordinated Vi (compare monomer spectra from Figs. 3 and 6). Comparison of Fig. 8 with Figs. 3 and 6 suggests that the coordination of the optically active vanadate center in MnVi-S1 or CoVi-S1 is tbp. MgVi-S1, NiVi-S1, FeVi-S1, and CaVi-S1 did not

develop an observable CD signal in the lowest energy absorption band of the vanadate.

We observed the vanadate center CD spectrum from CoVi-S1 as a function of free vanadate concentration ranging from 0.2 to 1.0 mM (data not shown). In this range, monomeric, dimeric and tetrameric vanadate species are present at known concentrations [30]. CD from the tbp-coordinated model compounds indicate that bound vanadate stoichiometry does not influence the shape of the CD spectrum; however, signal intensity from CoVi-S1 scales linearly only with tetrameric vanadate concentration, indicating that it originates principally from tetravanadate binding to S1. We propose that the optically active vanadate occupies the γ-phosphate location in the ATP binding site, a location indicated by the vanadate-mediated photocleavage in these complexes described in Section 3.4 below, and that the induced signal follows from specific interactions between the oxygen ligands of Vi and the active site of S1.

Myosin S1 complexed with MeADPVi also develops a strong extrinsic cotton effect in the absorption band of the vanadate. Fig. 9 shows the vanadate center CD spectrum of MgADPVi-S1. Comparison of Fig. 9 with Figs. 3 and 6 suggest that the coordination of the vanadate center in MgADPVi-S1 is Oh. Similar spectra were observed from the vanadate center when the complex was formed with the divalent metal cations Mn^{2+}, Co^{2+}, Ni^{2+}, Fe^{2+}, and Ca^{2+}. The appearance of the CD band around 350 nm is very characteristic to the MeADPVi-S1 complex, while its intensity and wavelength maximum depend on the specific metal cation. Table 1 summarizes the rotary strengths and wavelength maxima for this electronic transition in MeADPVi-S1 as a function of the divalent cation. We find that the rotary strengths correlate with V_{max} of the actin-activated ATPase for the various divalent cations, except for Ni^{2+} [11], probably because Ni^{2+} has square planar geometry unlike the other metals, which have octahedral or tetrahedral geometry.

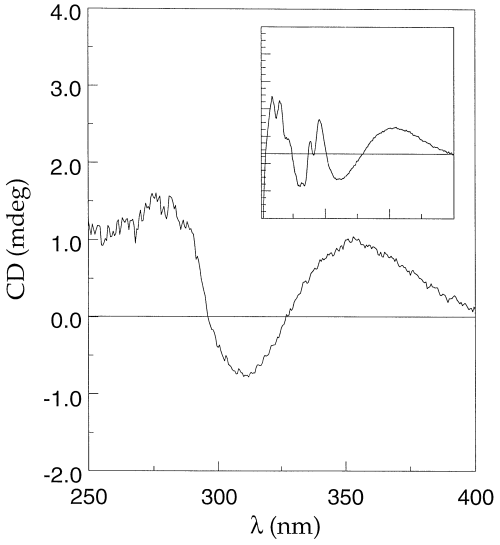

Fig. 9. The CD difference spectra between MgADPVi-S1 and MgADP-S1. The insert shows the MgADPVi-S1 spectrum after subtraction of the free MgADP signal. The axes in the inset are scaled identically to those in the larger figure. The spectrum in the insert is identical to that produced from an equal protein concentration sample of MgADPVi-S1 when free MgADP was removed by gel filtration. Spectra were measured in a 0.5 cm cell.

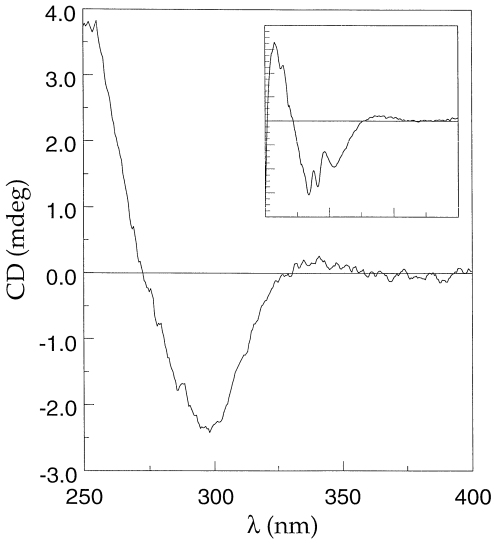

Fig. 8. The CD difference spectra between CoVi-S1 and Co-S1. The insert shows the CoVi-S1 spectrum before subtraction. The axes in the insert are scaled identically to those in the larger figure. Spectra were measured in a 0.5 cm cell.

3.4. Vanadate-induced photocleavage of MeVi-S1

Irradiation with near UV light in the presence of MgVi cleaves the S1 heavy chain at three specific sites viz., at 23, 31 and 74 kDa from the N-terminus

Table 1
The effect of divalent cations on the wavelength maxima and rotary strength of the lowest energy electronic transition of the MeADPVi-S1 complex and on the actin-activated ATPase

Metal	λ_{max} (nm)	Rotary Strength (D–B)	V_{max} actin-activated ATPase (s^{-1})[a]
Mn^{2+}	344	0.12	16.4
Mg^{2+}	348	0.105	14.7
Ni^{2+}	353	0.056	3.1
Co^{2+}	345	0.041	10.8
Fe^{2+}	341	0.041	8.1
Ca^{2+}	346	0.025	7.1

[a] Values measured at 25°C and taken from Peyser et al. [11].

[30,34]. The 23- and 31-kDa cleavage sites are at Ser180 [35] and Ser242 [36], respectively, and both sites were shown to participate in forming a phosphate binding loop in the active site of myosin [14], demonstrating Vi binding to the active site. Since only MnVi-S1 and CoVi-S1 produce characteristic vanadate center CD signals, we UV-irradiated MeVi-S1 samples and analyzed the products with SDS-PAGE to test whether MnVi and CoVi bind to the active site. Our results are shown in Fig. 10.

UV irradiated samples of S1 heavy chain are cleaved at 23 kDa from the N-terminus in the presence of Mn^{2+} and Co^{2+}. Increasing divalent cation up to 5 mM has no effect on the 23-kDa cleavage, even though this cation concentration partially inhibits the photocleavage at 74 kDa from the N-terminus (see also Ref. [37]). In contrast, the presence of Mn^{2+}, and even more so Co^{2+}, inhibited the cleavage at the 31 kDa site. These results indicate that the phosphate binding loop of the active site is occupied by vanadate in the presence of MnVi or CoVi; however, the binding is different from the binding of MgVi, where there is cleavage at both sites. The difference in the bound vanadate structure between MnVi-S1 or CoVi-S1 and MgVi-S1, suggested by photocleavage, is also indicated by CD where a vanadate center CD signal originates from MnVi-S1 and CoVi-S1, but not from MgVi-S1 or from the other MeVi-S1 complexes used in this study.

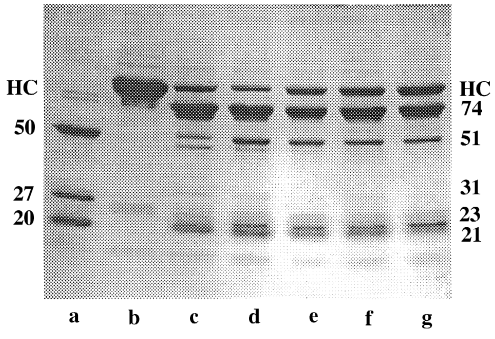

Fig. 10. Vanadate-induced photocleavage of MnVi-S1 and CoVi-S1. Vi in 0.5 mM concentration was added to 8 μM S1 in 30 mM HEPES pH 7.0 and increasing concentrations of $MnCl_2$ or $CoCl_2$. The samples were irradiated by UV light and analyzed by SDS-PAGE as described in Section 2. Lanes: (a) tryptic S1; (b) S1; (c) irradiated S1, 2 mM $MgCl_2$; (d) irradiated S1, 0.5 mM $MnCl_2$; (e) irradiated S1, 5.0 mM $MnCl_2$; (f) irradiated S1, 0.5 mM $CoCl_2$; (g) irradiated S1, 5.0 mM $CoCl_2$. Vertical letters: HC, S1 heavy chain (95 kDa). Left vertical numbers: molecular masses of tryptic S1 heavy chain fragments in kilodaltons. Right vertical numbers: molecular masses of the S1 heavy chain fragments produced by photocleavage in kilodaltons.

3.5. Calculation of optical signals

We calculated the energy, and dipole and rotary strengths of electronic transitions in model monomeric cyclic esters of vanadate in tbp and Oh coordination geometry as described in Appendix B. Fig. 11 shows the observed $\Delta\epsilon_M$ from Fig. 3 for the monomeric *R*-propanediol–Vi cyclic ester in the tbp coordination geometry. The transition energies and rotary strengths measured from $\Delta\epsilon_M$ are also shown in the figure as are the estimates made from the semi-empirical calculations on model monomeric tbp structures (taken from the dimeric cyclic ester shown in the insert to Fig. 3). We considered two isomers for the monomeric cyclic ester, where the methyl group on the propanediol is closest to, either the oxygen at an apex of one of the bipyramids, or an

oxygen in the plane of the common base of the bipyramids. We calculated similar rotary strengths and identical transition energies for these isomers, and averaged their rotary strengths to arrive at the estimate shown in Fig. 11. We did not attempt to compare observed and calculated dipole strengths because with absorption, the contributions from cyclic ester monomers and dimers, the various acyclic esters, and vanadate are not readily distinguishable as they are with CD.

Fig. 12 shows the observed $\Delta\epsilon_M$ from Fig. 6 for the monomeric *S*-lactate–Vi cyclic ester in the Oh coordination geometry. The transition energies and rotary strengths measured from $\Delta\epsilon_M$ are shown in the figure, as are the estimates made from the semi-empirical calculations on a model monomeric Oh structure (shown in the inset to Fig. 6). The model tbp and Oh structures give energies and rotary strengths in good qualitative agreement with the observed values.

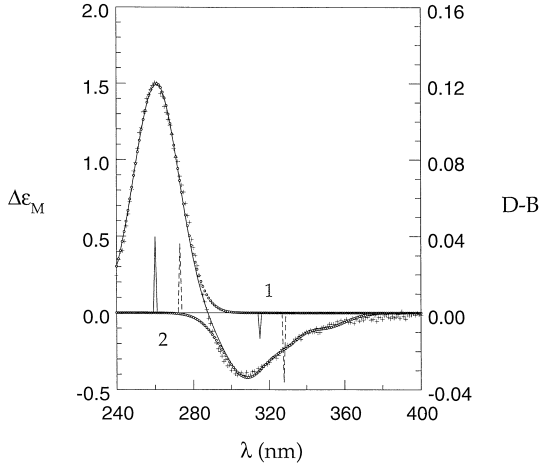

Fig. 11. The observed $\Delta\epsilon_M$ (+ + +) for the *R*-propanediol–Vi cyclic ester in the tbp coordination geometry taken from Fig. 3. The spectrum consists of two electronic transitions best fitted with a sum of four Gaussian curves (solid line). A single positive amplitude Gaussian curve (◦ ◦ ◦) approximates the higher energy transition centered at 260 nm. A sum of three negative amplitude Gaussian curves (◦ ◦ ◦) approximate the lower energy transition centered at 315 nm. The scale on the right *y*-axis is in Debye–Bohr Magneton (D–B) for comparison with the height of the solid or broken vertical spikes in the figure. The height of the solid (broken) spike is the rotary strength observed (calculated) for each electronic transition. The position of the solid (broken) vertical spikes on the abscissa represents the observed (calculated) transition energies. Comparable observed and calculated transitions are grouped under transition number 1 or 2 designated in the figure.

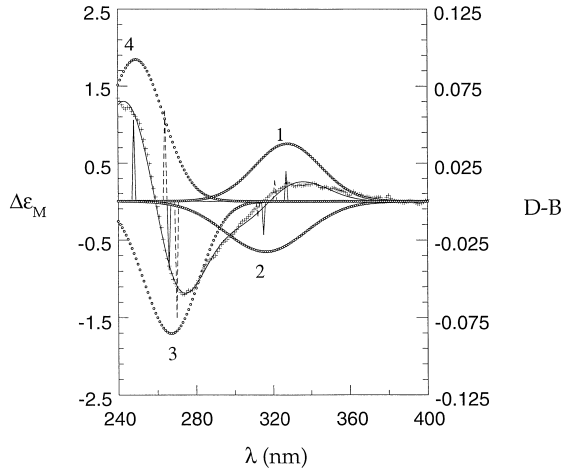

Fig. 12. The observed $\Delta\epsilon_M$ (+ + +) for the *S*-lactate–Vi cyclic ester in the Oh coordination geometry taken from Fig. 6. The spectrum consists of four electronic transitions best fitted with a sum of four Gaussian curves (solid line). The two positive amplitude Gaussian curves (◦ ◦ ◦) approximate the transitions centered at 248 and 327 nm. The two negative amplitude Gaussian curves (◦ ◦ ◦) approximate the transitions centered at 266 and 315 nm. The vertical spikes are for comparison of observed (solid) and calculated (broken) electronic transition energies and rotary strengths as described in the caption to Fig. 11. Comparable observed and calculated transitions are grouped under transition numbers 1, 2, 3, or 4 designated in the figure.

4. Discussion

The coupling of chemical intermediates in ATP hydrolysis with transient structural states of myosin S1 in contraction is a practical model for energy transduction that can be investigated using structural studies of the bound ATP and S1. ATP hydrolysis, from the viewpoint of ATP structure, might be described as a lengthening of the distance, *d*, separating Pγ from the oxygen connecting the γ- and β-phosphates [2], while γ-phosphate coordination geometry shifts from tetrahedral to tbp [1]. The protein responds to the ATP structural changes with its own structural changes that we characterize generally as performing energy transduction. The transient state analogs provide a means to study both protein and nucleotide structures if the analog faithfully repre-

sents the principal structural features of the real ATPase intermediates. Lately, we used the movement of the probe binding cleft, in response to the trapping of the phosphate analogs, to support the notion that an increase in *d* correlates with closure of the probe binding cleft [2,16]. This previous work established that the phosphate substitutes such as, beryllium fluoride, aluminum fluoride, scandium fluoride, and vanadate mimic the real ATP transient with regard to *d*.

A second interesting aspect of the ATP transient analog is its coordination geometry, and how well the vanadate can mimic the native structure of the terminal phosphate. The vanadium (V) anion has a more flexible coordination geometry than phosphate [38,39]. Tetra, penta, and hexacoordinated vanadate molecules have various stereostructures that depend on concentration, pH, and complexing agents. These structures were studied from vanadate complexes in solution, bound to proteins, and in crystal form producing a variety of sometimes divergent results [18–23,33,40–42], possibly due to differences in methods, interpretation, or in hydration of the vanadate complex in solution vs. the solid state.

In this paper, we investigated the coordination geometry of the vanadate phosphate analog of an ATP transient using CD. This is possible with the vanadate, because its lowest energy electronic transitions are in a region of the spectrum distinct from the contribution of the protein. We verified, using biomimetic model compounds of vanadate cyclic esters in solution, that the vanadate CD signal in these absorption bands uniquely distinguishes the tbp from the Oh coordination geometry. Then, upon comparison of model spectra with spectra from MgADPVi-S1, we concluded that trapped vanadate in MgADPVi-S1 is in the Oh coordination geometry. Vi trapped in *Dictyostelium* S1 was reported to be in the tbp coordination [15]. This discrepancy could be from several possibilities including, structural differences between the truncated *Dictyostelium* and rabbit skeletal S1 that affect substrate binding [25,26], or differences between crystal and solution structures [23,42]. The latter possibility may be from the involvement of a water molecule in the solution structure that changes the vanadate geometry from penta to hexacoordination. Comparison of model spectra with Co or MnVi-S1 spectra indicates that the vanadate center in these species have tbp coordination geometry. The scaling of the CD signal in Co or MnVi-S1 with the concentration of the free tetravanadate species in solution suggests that Vi binds to the active site of myosin in the tetrameric form in agreement with previous ^{51}V-NMR results [30,37].

The docking of the vanadate center in the MgADPVi-S1 complex is at the γ-phosphate site. Bound MeVi is a tetramer, and probably part of it binds to S1 similarly to Mg-pyrophosphate. The vanadate stabilizing side chains are likely the serine OH groups (serine-180 and 243) as shown by vanadate-induced photocleavage of S1 in MeVi-S1 [30,34,37,43,44] and by the X-ray structure of the ATP binding site [15]. These connections are very similar to those formed in the biomimetic vanadate models if we substitute the serine OH groups with the vicinal OHs of the propanediol. The biomimetic models suggest that the tbp vanadate structure in the protein is formed by esterification with alcoholic OH groups from these serines. The Oh coordination needs an additional ligand possibly formed with a water molecule, and, different stabilizing connections perhaps with one of the carboxyl groups in the γ-phosphate site.

Both the Vi-induced photocleavage and Vi center CD experiments demonstrated metal cation dependence in the interaction between Vi and the active site of S1. In the photocleavage experiments, the optically inactive MgVi-S1 complex was cleaved at Ser180 and Ser243 while the optically active CoVi-S1 and MnVi-S1 complexes were cleaved only at Ser180. In MeADPVi-S1 complexes the active site of MgADPVi-S1 is cleaved at Ser180, but not when Co^{2+}, Mn^{2+}, or Ni^{2+} is the accompanying cation [45], and, the rotary strength and wavelength maximum of the Vi CD band in MeADPVi-S1 depends on the cation present. Most significantly, the correlated cation dependence of V_{max} in actin-activated ATPase with the vanadate rotary strength in MeADPVi-S1 (see Table 1), relates a biochemical property of the native substrate with the detailed geometry of the Oh coordination of the vanadate analog. Probably, the fact that the metal cation interacts with the functionalities of both the active site and substrate [14], while these interactions are affected by the coordination geometry and the ionic radius of the divalent metal, is why the binding of vanadate is

influenced by the nature of the accompanying metal cations. This influence similarly appears in the ATPase [11].

Our past and present work suggests that the trapped vanadate analog of the ATPase intermediate in S1 reliably mimics one proposed feature of the real intermediate, i.e., the length *d* that correlates with closure of the probe binding cleft [2], but fails to mimic a second proposed feature of the real intermediate, i.e., the tbp coordination of the -phosphate. There are two scenarios for the implications of these findings for the mechanism of energy transduction. The first is that the trapped vanadate analog is an incomplete representation of an ATPase intermediate as recently suggested for ribonuclease A [46], and for rabbit S1, since its coordination geometry is not tbp as expected from earlier work on other enzymes [33,40] and *Dictyostelium* S1 [15]. The second is that the trapped vanadate analog represents a transient Oh structure of the terminal phosphate in S1 ATPase similar to the structure of the fluoraluminates trapped in NTPase enzymes [14,47,48]. Let us assume in the subsequent discussion that both *d* and the coordination geometry of the γ-phosphate are important in energy transduction.

If the first scenario is correct, then it appears that S1 structure responds to ATP hydrolysis in two or more independent ways. One response, due to changing *d*, is elicited by the vanadate analog and causes closure of the probe binding cleft, while perhaps another unmonitored response, for instance actin-binding affinity modulation, is controlled by γ-phosphate coordination, and does not occur with this analog. If the second scenario is correct, then an Oh coordinated γ-phosphate is a transient intermediate of ATP hydrolysis. This notion is supported by the divalent cation-mediated correlation between the V_{max} of actin-activated ATPase and the rotary strength of the vanadate analog. The Oh coordination of the phosphate atom was demonstrated with model compounds [3,4]; however, the literature on nucleotide transient intermediates in RNAse [18,33,40] do not mention this possibility. The application of our optical technique to other vanadate-trapped ATPases may provide further evidence supporting one of the two scenarios, or, show that the use of the Oh coordination in ATPase is enzyme-dependent. The latter idea is supported by the ability of trapped Al to assume tbp or Oh coordinations in different enzymes including myosin [14], nucleoside diphosphate kinase [49], and GTPase-activating protein [50].

In summary, comparison of CD spectra originating from model vanadate compounds of known structure to that obtained from the vanadate-S1 complex identified the structure of the vanadate center in S1. Contrary to expectations, the vanadate center in S1-trapped MgADPVi is octahedral, raising questions about the competence of the vanadate as a transient state analog for ATP hydrolysis. Trapped vanadate CD from other ATPases may help to clarify if the present observations are unique to myosin.

Acknowledgements

We thank Dr. Nenad Juranic of the Mayo NMR Core Facility for making the ^{51}V-NMR measurements. The comments of a reviewer are also appreciated. This work was supported by grants from the National Institutes of Health (R01 AR 39288), the American Heart Association (GIA 930 06610), and the Mayo Foundation.

Appendix A. Equilibrium constants, $\Delta\epsilon_M$, and $\Delta\epsilon_D$ from mixtures of propanediol or lactate with Vi

A.1. Propanediol–Vi

We model the mixture of propanediol and Vi with the scheme suggested for ethylene glycol–Vi mixtures [19,21],

$$\mathrm{Vi} + \mathrm{T} \overset{K_1}{\rightleftarrows} \mathrm{A} + \mathrm{W} \quad (A1)$$

$$\mathrm{A} + \mathrm{T} \overset{K_2}{\rightleftarrows} \mathrm{B} + \mathrm{W} \quad (A2)$$

$$\mathrm{A} \overset{K_3}{\rightleftarrows} \mathrm{M} \quad (A3)$$

$$\mathrm{A} + \mathrm{A} \overset{K'_3}{\rightleftarrows} \mathrm{D} + 2\mathrm{W} \quad (A4)$$

$$\mathrm{M} + \mathrm{M} \overset{K_4}{\rightleftarrows} \mathrm{D} + 2\mathrm{W} \quad (A5)$$

where K_is are equilibrium constants, Vi is free

vanadate, T is propanediol, W is water, A is an acyclic ester of vanadate, and B is an acyclic diester. The M and D species are the optically active monomer and dimer cyclic esters introduced in Eq. (1). We solve for [M] and [D] in terms of the equilibrium constants and the total vanadate concentration, $[Vi]_T = [Vi] + [A] + [B] + [M] + 2[D]$, finding,

$$[M] = 2x\left[-1 + (1 + y[Vi]_T)^{1/2}\right]/y \quad (A6)$$

$$[D] = 1/2\left[-1 + (1 + y[Vi]_T)^{1/2}\right]^2/y \quad (A7)$$

with

$$y = 4a/b^2 \qquad x = 1/b \quad (A8)$$

$$a = 2K_4/[W]^2 \quad b = 1 + \frac{1}{\gamma K_1 K_3} + \frac{1}{K_3} + \frac{\gamma K_2}{K_3} \quad (A9)$$

$$\gamma \equiv [T]/[W] \quad (A10)$$

[W] and [T] are treated as constant because they are in large excess of the other molecules in all of the experiments. The equilibrium constants K_1 and K_2 describe the esterification of vanadate with propanediol. They were measured for the vanadate/ethylene glycol mixture to be 18.6 ± 1.0 and 4.9 ± 0.31, respectively [19], and have comparable values in other vanadate/alcohol mixtures [51].

In propanediol–Vi $\Delta\epsilon_M$ and $\Delta\epsilon_D$ are equal except for scaling factors such that the wavelength dependence in the CD signal can be isolated using, $S(\lambda,[Vi]_T, \gamma) = s([Vi]_T, \gamma)g(\lambda)$, $\Delta\epsilon_M = e_M g(\lambda)$, and $\Delta\epsilon_D = e_D g(\lambda)$, where $g(\lambda)$ is the shape function. The relationship among the unknowns are then, from Eqs. (1), (A6), (A7), (A8), (A9) and (A10),

$$s([Vi]_T,\gamma)/\ell = 32\,980\left\{e_M 2x\left[-1 + (1 + y[Vi]_T)^{1/2}\right]/y + e_D^{1/2}\left[-1 + (1 + y[Vi]_T^{1/2}\right]^2/y\right\} \quad (A11)$$

Eqs. (A8), (A9), (A10) and (A11) show that the $[Vi]_T$ and γ dependence in $s([Vi]_T, \gamma)$ is explicit in $[Vi]_T$ but implicit in γ. We used $s([Vi]_T, \gamma)$ for $\gamma = 0.0047$ ($[T]/[W] = 0.263/55.556$) and $12.5\ \mu M \le [Vi]_T \le 350\ \mu M$ and solved the system of Eq. (A11) for unknowns xe_M, e_D, and y with a linear least squares protocol for linear parameters xe_M and e_D, while varying y over all possible values. The best fit requires,

$$x(\gamma = 0.00475)\, e_M = 0.30\,(M\,cm)^{-1} \quad (A12)$$

$$e_D = 17.6\,(M\,cm)^{-1} \quad (A13)$$

$$y(\gamma = 0.00475) = 2.0 \times 10^3\ M^{-1} \quad (A14)$$

We observed $s([Vi]_T, \gamma)$ for $[Vi]_T = 200\ \mu M$ and $3.6 \times 10^{-4} \le \gamma \le 3.2 \times 10^{-3}$ (data not shown) and solved the system of Eq. (A11) for unknowns e_M, K_1, K_2, and K_3 subject to the constraints in Eqs. (A12), (A13) and (A14). We find that Eqs. (A11), (A12), (A13) and (A14) are insensitive to the choice of K_2 because γ is always small in our conditions (see Eq. (A9)), and we may assume $K_2 \approx 4.9$, its value for ethylene glycol, without significantly affecting the other parameters in the solution set. The best fit then requires $e_M = 1.4\ (M\,cm)^{-1}$, $K_1 = 18.6$, $K_3 = 3.5$, $K_4/[W] = 2.8 \times 10^5$, $K_3' = K_4 K_3^2/[W] = 3.5 \times 10^6$, and the $\Delta\epsilon_M$ and $\Delta\epsilon_D$ plotted in Fig. 3.

K_1 is identical to, while K_3' is larger than, the equivalent values for the ethylene glycol case [K_3 and K_4 were not determined and $K_3' = 2.3$–2.6×10^5 in the ethylene glycol/vanadate system [19]]. This result for K_3', indicating that the propanediol–Vi mixture forms more cyclic esters than a comparable mixture of ethylene glycol–Vi, was confirmed with ^{51}V-NMR (data not shown).

A.2. Lactate–Vi

The ^{51}V-NMR from lactate and Vi at pH 6.1 in Fig. 1 shows that the mixture contains cyclic esters of lactate–Vi but no other species. The relevant scheme describing this system is Eq. (A5) for the combination of monomeric and dimeric cyclic esters with equilibrium constant K_4, except that only one water molecule is liberated with dimer formation [24]. We solved this problem using lactate–Vi CD spectra observed as a function of $[Vi]_T$ to find $\Delta\epsilon_M$,

$\Delta\epsilon_D$ and K_4 by a method described previously for the analogous problem of dimer formation in xanthene dyes [52]. We find $K_4 = 2.7 \times 10^5$ and the $\Delta\epsilon_M$ and $\Delta\epsilon_D$ plotted in Fig. 6.

Appendix B. Energies, dipole and rotary strengths of the tbp and Oh coordinated vanadate

All possible structural isomers of the *R*-propanediol–Vi cyclic ester monomer were generated and energy minimized in vacuum using molecular mechanics (MM+ force field). The starting bond distances and angles for tbp-coordinated Vi were taken from the crystal structure [20]. The *S*-lactate–Vi cyclic ester was similarly generated and energy minimized, but no crystal structure was available for this model compound. The absorption spectra of the energy-minimized isomers were calculated with the semi-empirical quantum mechanical method ZINDO/S with configuration interaction (CI) and parameterization for spectroscopy from transition metals [53]. ZINDO/S calculations were carried out on the cyclic esters with a charge of -1 and zero electronic spin in the ground state. We computed rotary strengths for these molecules from Hartree–Fock radial wavefunctions and atomic orbital coefficients generated in ZINDO/S using the origin independent matrix method [54,55] as described below.

The ZINDO/S calculation combines atomic orbitals, $|\phi_i\rangle$, to produce coefficients, $C_{i,j}$, giving molecular orbitals $|\psi_i\rangle = \sum_\mu C_{\mu,i}|\phi_\mu\rangle$ describing the electronic structure of the molecule. The sum over μ in $\sum_\mu C_{\mu,i}|\phi_\mu\rangle$ covers all of the atomic orbitals in the basis set. The CI diagonalizes the Hamiltonian operator with molecular orbitals producing energy eigenvalues and the CI molecular orbital coefficients, $D_{i,j}$, giving the state wavefunctions $|\Phi_i\rangle = \sum_\mu D_{\mu,i}|\psi_\mu\rangle$. We choose occupied and unoccupied molecular orbitals to participate in the CI, so that the sum over μ in $\sum_\mu D_{\mu,i}|\psi_\mu\rangle$ covers only the participating orbitals. We find the electron density matrix elements, $\mathbf{P}_{\mu,\nu}(j \leftarrow i)$, using the relation,

$$\langle\Phi_j|\hat{c}|\Phi_i\rangle = \sum_{\mu,\nu} P_{\mu,\nu}(j \leftarrow i)\langle\phi_\mu|\hat{c}|\phi_\nu\rangle \qquad \text{(B1)}$$

where $\hat{c}$ is an arbitrary operator. Substituting on the left hand side of Eq. (B1) with $|\Phi_i\rangle = \sum_{\mu,\nu} D_{\mu,i}C_{\nu,\mu}|\phi_\nu\rangle$, we construct the density matrix from the known coefficients $D_{i,j}$ and $C_{i,j}$. The neglect of diatomic differential overlap approximation simplifies Eq. (B1), such that the sums over μ and ν pertain only to atomic orbitals from a given atom A. This is indicated by a superscript on **P** and the explicit sum over atoms, giving

$$\langle\Phi_i|\hat{c}|\Phi_i\rangle = \sum_A \sum_{\mu,\nu} P^A_{\mu,\nu}(j \leftarrow i)\langle\phi_\mu|\hat{c}|\phi_\nu\rangle \qquad \text{(B2)}$$

The electric and magnetic dipole moment matrix elements for a molecule, $\langle\Phi_f|\mathbf{e}|\Phi_i\rangle$ and $\langle\Phi_i|\mathbf{m}|\Phi_f\rangle$, are from Eq. (B2),

$$\langle\Phi_f|\mathbf{e}|\Phi_i\rangle = \sum_A \sum_{\mu,\nu} P^A_{\mu,\nu}(f \leftarrow i)\, q\langle\phi_\mu|\mathbf{R}_A|\phi_\nu\rangle \qquad \text{(B3)}$$

$$\langle\Phi_i|\mathbf{m}|\Phi_f\rangle = \sum_A \sum_{\mu,\nu} P^A_{\mu,\nu}(i \rightarrow f)\,\langle\phi_\mu|\mathbf{R}_A \times \boldsymbol{p}|\phi_\nu\rangle \qquad \text{(B4)}$$

where q is the charge of an electron, $\boldsymbol{R}_A$ is the position vector of an electron in an orbital of atom A, and $\boldsymbol{p}$ is the momentum operator of an electron (you need not specify A on $\boldsymbol{p}$ since this operator is the same for every atom). Substituting the expression $\boldsymbol{R}_A = \boldsymbol{R}_{A,0} + \mathbf{r}$, where $\boldsymbol{R}_{A,0}$ is the vector from the origin to the nucleus of atom A, and $\mathbf{r}$ is the vector from the nucleus to the electron, into Eqs. (B3) and (B4) gives,

$$\langle\Phi_f|\mathbf{e}|\Phi_i\rangle = \sum_A \left\{ R_{A,0}\left[Z_A - \sum_\mu P^A_{\mu,\mu}(f \leftarrow i)\right] + \sum_{\mu,\nu} P^A_{\mu,\nu}(f \leftarrow i)\, q\langle\phi_\mu|\mathbf{r}|\phi_\nu\rangle \right\} \qquad \text{(B5)}$$

$$\langle\Phi_i|\mathbf{m}|\Phi_f\rangle = \frac{(-1)^{1/2}\pi(E_i - E_f)}{hc}\sum_A \mathbf{R}_{A,0} \times\langle\Phi_i|\mathbf{e}|\Phi_f\rangle + (\beta/\hbar)\sum_A \sum_{\mu,\nu} P^A_{\mu,\nu}(i \rightarrow f)\langle\phi_\mu|\mathbf{L}|\phi_\nu\rangle \qquad \text{(B6)}$$

where Z_A is the nuclear charge of atom A, E_j is the energy eigenvalue associated with $|\Phi_j\rangle$, β is the Bohr Magneton, $\hbar$ is Planck's constant divided by 2π, **L** is the orbital angular momentum operator, and c is the speed of light. The step from Eqs. (B4), (B5)

and (B6) uses the substitution $\langle \Phi_i|\mathbf{p}|\Phi_j\rangle = [(-1)^{1/2} m/\hbar](E_i - E_j)\langle \Phi_i|\mathbf{r}|\Phi_j\rangle$. The electric dipole moment is the sum of the classical electric dipole moment and the polarization of the atomic orbitals. The magnetic dipole moment is the sum of the origin-independent extrinsic magnetic dipole and the intrinsic magnetic dipole neglecting electronic spin.

We compute the dipole and rotary strengths for transitions from the ground state using the formulas [56],

$$D_{0,f} = |\langle \Phi_f|\mathbf{e}|\Phi_0\rangle|^2 = 9.18 \times 10^{-3} n\rho^2 \int \epsilon \, d\lambda/\lambda \qquad D^2 \qquad (B7)$$

$$R_{0,f} = \mathrm{Im}\{\langle \Phi_f|\mathbf{e}|\Phi_0\rangle \cdot \langle \Phi_0|\mathbf{m}|\Phi_f\rangle\} = 0.248 \rho \int \Delta\epsilon \, d\lambda/\lambda \qquad D\text{–}B \qquad (B8)$$

where n is the index of refraction of the medium containing the light absorbing molecule, $\rho = 3/(n^2 + 3)$ is the Lorentz correction accounting for the polarizability of the solvent, Im means take the imaginary part, D is Debye, and D–B is the Debye–Bohr Magneton.

References

[1] M. Chabre, TIBS 15 (1990) 6.
[2] S. Park, K. Ajtai, T.P. Burghardt, Biochemistry 36 (1997) 3368.
[3] F. Ramirez, K. Tasaka, N.B. Desai, C.P. Smith, J. Am. Chem. Soc. 90 (1968) 751.
[4] W.C. Archie Jr., F.H. Westheimer, J. Am. Chem. Soc. 95 (1973) 5955.
[5] C.C. Goodno, Proc. Natl. Acad. Sci. U.S.A. 76 (1979) 2620.
[6] K. Ajtai, L. Szilagyi, E.N.A. Biro, FEBS Lett. 141 (1982) 74.
[7] B. Phan, E. Reisler, Biochemistry 31 (1992) 4787.
[8] M.M. Werber, Y.M. Peyser, A. Muhlrad, Biochemistry 31 (1992) 7190.
[9] B.C. Phan, L.D. Faller, E. Reisler, Biochemistry 32 (1993) 7712.
[10] G.D. Henry, S. Maruta, M. Ikebe, B.D. Sykes, Biochemistry 32 (1993) 10451.
[11] Y.M. Peyser, M. Ben-Hur, M.M. Werber, A. Muhlrad, Biochemistry 35 (1996) 4409.
[12] Y.M. Peyser, K. Ajtai, M.M. Werber, T.P. Burghardt, A. Muhlrad, Biochemistry 36 (1997) 5170.
[13] D. Gopal, M. Burke, J. Biol. Chem. 270 (1995) 19282.
[14] A.J. Fisher, C.A. Smith, J.B. Thoden, R. Smith, K. Sutoh, H.M. Holden, I. Rayment, Biochemistry 34 (1995) 8960.
[15] C.A. Smith, I. Rayment, Biochemistry 35 (1996) 5404.
[16] S. Park, K. Ajtai, T.P. Burghardt, Biochim. Biophys. Acta 1296 (1996) 1.
[17] B.C. Phan, Y.M. Peyser, E. Reisler, A. Muhlrad, Eur. J. Biochem. 243 (1997) 636.
[18] M. Krauss, H. Basch, J. Am. Chem. Soc. 114 (1992) 3630.
[19] M.J. Gresser, A.S. Tracey, J. Am. Chem. Soc. 108 (1986) 1935.
[20] T.W. Hambley, R.J. Judd, P.A. Lay, Inorg. Chem. 31 (1992) 343.
[21] W.J. Ray Jr., D.C. Crans, J. Zheng, J.W. Burgner II, H. Deng, M. Mahroof-Tahir, J. Am. Chem. Soc. 117 (1995) 6015.
[22] S.E. Harnung, E. Larsen, E.J. Pedersen, Acta Chem. Scand. 47 (1993) 674.
[23] S.J. Angus-Dunne, R.J. Batchelor, A.S. Tracey, F.W.B. Einstein, J. Am. Chem. Soc. 117 (1995) 5292.
[24] A.S. Tracey, M.J. Gresser, K.M. Parkinson, Inorg. Chem. 26 (1987) 629.
[25] S.K.A. Woodward, M.A. Geeves, D.J. Manstein, Biochemistry 34 (1995) 16056.
[26] A.A. Bobkov, K. Sutoh, E. Reisler, J. Muscle Res. Cell Motil. 18 (1997) 563.
[27] C.C. Goodno, Methods Enzymol. 185 (1982) 116.
[28] Y. Tonomura, P. Appel, M.F. Morales, Biochemistry 5 (1966) 515.
[29] A.G. Weeds, R.S. Taylor, Nature 257 (1975) 54.
[30] I. Ringel, Y.M. Peyser, A. Muhlrad, Biochemistry 29 (1990) 9091.
[31] G. Strang, Introduction to Applied Mathematics, Wellesley-Cambridge Press, Wellesley, MA, 1986.
[32] E.L. Eliel, S.H. Wilen, Stereochemistry of Organic Compounds, Wiley, New York, 1994.
[33] A. Wlodawer, M. Miller, L. Sjolin, Proc. Natl. Acad. Sci. U.S.A. 80 (1983) 3628.
[34] A. Muhlrad, Y.M. Peyser, I. Ringel, Biochemistry 30 (1991) 958.
[35] C.R. Cremo, J.C. Grammer, R.G. Yount, J. Biol. Chem. 264 (1989) 6608.
[36] J.C. Grammer, R.G. Yount, Biophys. J. 59 (1991) 226a.
[37] C.R. Cremo, G.T. Long, J.C. Grammer, Biochemistry 29 (1990) 7982.
[38] R.R. Holmes, Pentacoordinated Phosphorus Vol. 1: Structure and Spectroscopy, Am. Chem. Soc., Washington, DC, 1980.
[39] A. Butler, in: N.D. Chasteen (Ed.), Vanadium in Biological Systems, Kluwer Academic Publishers, Dordrecht, 1990, p. 25.
[40] B. Borah, C. Chen, W. Egan, M. Miller, A. Wlodawer, J.S. Cohen, Biochemistry 24 (1985) 2058.
[41] P. Caravan, L. Gelmini, N. Glover, F.G. Herring, H. Li, J.H. McNeill, S.J. Rettig, I.A. Setyawati, E. Shuter, Y. Sun, A.S. Tracey, V.G. Yuen, C. Orvig, J. Am. Chem. Soc. 117 (1995) 12759.
[42] D.C. Crans, H. Chen, O.P. Anderson, M.M. Miller, J. Am. Chem. Soc. 115 (1993) 6769.
[43] C.R. Cremo, J.C. Grammer, R.G. Yount, Methods Enzymol. 196 (1991) 442.

[44] J.C. Grammer, J.A. Loo, C.G. Edmons, C.R. Cremo, R.G. Yount, Biochemistry 35 (1996) 15582.
[45] J.C. Grammer, C.R. Cremo, R.G. Yount, Biochemistry 27 (1988) 8408.
[46] C.H. Leon-Lai, M.J. Gresser, A.S. Tracey, Can. J. Chem. 74 (1996) 38.
[47] J. Sondek, D.G. Lambright, J.P. Noel, H.E. Hamm, P.B. Sigler, Nature 372 (1994) 276.
[48] E.J. Martinez, J.L. Girardet, C. Morat, Inorg. Chem. 35 (1996) 706.
[49] Y.W. Xu, S. Morera, J. Janin, J. Cherfils, Proc. Natl. Acad. Sci. U.S.A. 94 (1997) 3579.
[50] K. Scheffzek, M.R. Ahmandian, W. Kabsch, L. Wiesmuller, A. Lautwein, F. Schmitz, A. Wittinghofer, Science 277 (1997) 333.
[51] A.S. Tracey, B. Galeffi, S. Mahjour, Can. J. Chem. 66 (1988) 2294.
[52] T.P. Burghardt, K. Ajtai, Biophys. Chem. 60 (1996) 119.
[53] W.P. Anderson, W. Edwards, M.C. Zerner, Inorg. Chem. 25 (1986) 2728.
[54] J.A. Schellman, E.B. Nielsen, J. Phys. Chem. 71 (1967) 3914.
[55] P.M. Bayley, E.B. Nielsen, J.A. Schellman, J. Phys. Chem. 73 (1969) 228.
[56] J.A. Schellman, Chem. Rev. 75 (1975) 323.